Tailoring the multipoles in THz toroidal metamaterials

Cong, Longqing; Srivastava, Yogesh Kumar; Singh, Ranjan

2017

Cong, L., Srivastava, Y. K., & Singh, R. (2017). Tailoring the multipoles in THz toroidal metamaterials. Applied Physics Letters, 111(8), 081108-.

https://hdl.handle.net/10356/85577

https://doi.org/10.1063/1.4993670

Tailoring the multipoles in THz toroidal metamaterials

Longqing Cong, Yogesh Kumar Srivastava, and Ranjan Singh[a)]
Division of Physics and Applied Physics, School of Physical and Mathematical Sciences, Nanyang Technological University, Singapore, Singapore 637371 and Centre for Disruptive Photonic Technologies, The Photonics Institute, Nanyang Technological University, Singapore, Singapore 637371

(Received 30 June 2017; accepted 5 August 2017; published online 23 August 2017)

The multipoles play a significant role in determining the resonant behavior of subwavelength resonators that form the basis of metamaterial and plasmonic systems. Here, we study the impact of multipoles including toroidal dipole on the resonance intensity and linewidth of the fundamental inductive-capacitance (LC) resonance of a metamaterial array. The dominant multipoles that strongly contribute to the resonances are tailored by spatial rearrangement of the neighboring resonators such that the mutual interactions between the magnetic, electric, and toroidal configurations lead to enormous change in the linewidth as well as the resonance intensity of the LC mode. Manipulation of the multipoles in a metamaterial array provides a general strategy for the optimization of the quality factor of metamaterial resonances, which is fundamental to its applications in broad areas of sensing, lasing and nonlinear optics where stronger field confinement plays a significant role. *Published by AIP Publishing.* [http://dx.doi.org/10.1063/1.4993670]

The discovery of metamaterials[1,2] led to an intense research activity in the recent decade in interdisciplinary areas including optics,[3] acoustics,[4] and heat.[5] Metamaterial is an artificially engineered array of subwavelength scale resonators that can be considered as a homogeneous medium described by the effective medium theory.[6] Several interesting phenomena have been observed by applying metamaterials for extraordinary manipulation of electromagnetic waves such as enhanced light-matter interaction,[7–10] perfect absorption,[11] and polarization control.[12] Most recently, the study of metasurfaces has shown bright prospects in designing planar, compact and high-efficiency devices for geometric optics.[13,14] A more complex supercell with a phase gradient or array with logically distributed resonators can give rise to an effective manipulation of wavefronts.[13,15,16]

The immense degree of freedom offered by metamaterials has enabled the design of three-dimensional (3D) meta-atoms, where a head-to-tail arrangement of magnetic dipoles gives rise to a measurable toroidal dipole.[17–21] Being first introduced by Zel'dovich,[22] toroidal dipole has been observed in the areas of nuclear and atomic physics,[23,24] solid state physics,[25] and classical electrodynamics.[26] The nonradiating feature of the toroidal geometry provides many interesting phenomena with enhanced light-matter interaction and applications in spaser,[27–30] ultrasensitive biosensing and nonlinear effects.[31–35] However, the fabrication complexity of 3D metamaterial at micro and nanoscale hinders the investigation of the toroidal dipole at higher frequencies.[36] In this context, the realization of toroidal dipole in a planar configuration[35,37–39] would provide an easy access to micro- and nano-optics regime. In this work, we experimentally demonstrate an enhanced coupling of Lorentzian inductive-capacitance (LC) resonance to the free space with a narrower linewidth by designing a symmetric supercell out of asymmetric single-split-ring resonators (ASRRs), where the electromagnetic multipoles including the in-plane toroidal dipole are tailored in a planar array of terahertz metamaterial resonators. We observe a drastic change in both the amplitude and the linewidth of the LC resonance by engineering the decomposed multipoles, which eventually leads to the optimization of the resonance properties.

A split ring resonator is usually designed symmetrically with the capacitive gap at the center of one arm of the square/circular resonator,[1] and an LC resonance is excited as the 1st order resonance mode with the incident electric field parallel to the gap arm. However, the LC mode remains dark for the orthogonally polarized excitation. Instead, a dipolar mode is induced due to the symmetry of the structure with respect to the incident field at a higher frequency. Here, we introduce a displacement of the split gap from the center of the resonator which breaks the structural symmetry with respect to y-axis. A linearly polarized incident wave along the y-axis will thus lead to a weak excitation of the fundamental LC resonance (see Fig. 1). We focus our observations on this weakly excited LC resonance and investigate the role of multipoles including the toroidal dipole that significantly impacts the nature of the ASRR resonance. We first study the weak LC resonance of ASRR in a uniform array denoted as S1, as shown in Fig. 1(a). The planar metamaterial samples were fabricated by using conventional photolithography, where the resonators were made of aluminum (200 nm thick) by thermal evaporation on a high-resistivity silicon substrate ($n = 3.43$) with a thickness of 500 μm. Detailed geometrical parameters are indicated in the caption of Fig. 1. A photoconductive antenna based terahertz time-domain spectroscopy system (THz-TDS) was used to measure the transmission spectra of the samples. The antennas are pumped and probed by two coherent femtosecond laser beams ($\sim$100 fs, 80 MHz repetition rate). Time domain signals were recorded by mapping the amplified photoconductive current that is proportional to the terahertz field, and then the frequency-domain spectra were extracted using the Fourier transform. Emitted radiation from the transmitter is linearly polarized and the

[a)]Email: ranjans@ntu.edu.sg

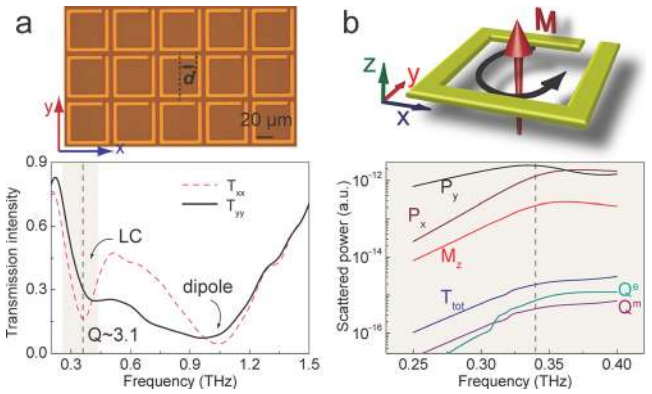

FIG. 1. The LC and dipole resonances in a uniform ASRR array (S1). (a) The fabricated ASRR array with measured transmission intensity spectra with *x*- and *y*-polarized incidence; geometric parameters of the unit cell are: square period 65 μm, square resonator length 50 μm and wire width 6 μm, gap width 3 μm and the gap displacement 17.5 μm. (b) Schematic illustration of an ASRR unit cell with the magnetic dipole excited at LC resonance with *y*-polarized excitation and the calculated scattered power of multipoles ($P_{x,y}$, electric dipole along *x*-/*y*-axis; M_z, magnetic dipole; $T_{x,y}$, toroidal dipole; Q^e, electric quadrupole; Q^m, magnetic quadrupole).

receiver is also polarization sensitive, so that the THz-TDS enables the detection of the orthogonal transmission responses of the samples, i.e., $\tilde{t}_{xx}$ and $\tilde{t}_{yy}$, by rotating the sample orthogonally. We present the normalized transmission intensity ($T(\omega) = |\tilde{t}_{sam}(\omega)/\tilde{t}_{ref}(\omega)|^2$) of the ASRR sample with the first two fundamental resonance modes in Fig. 1(a), where $\tilde{t}_{sam}(\omega)$ and $\tilde{t}_{ref}(\omega)$ are transmission amplitude of sample and reference, respectively. As indicated in the spectra, typical inductive-capacitive (LC) and dipole resonance modes are clearly captured for *x*-polarized excitation parallel to the gap arm. However, due to the non-centered capacitive gap of the ASRR, there is an extremely weak coupling of the LC mode to the *y*-polarized radiation resulting in a faint spectral footprint in the background of a broad dipolar resonance in T_{yy} spectrum.

To elucidate the nature of this fundamental mode, we performed a multipole analysis through calculating the simulated surface current excited by *y*-polarized incidence (see supplementary material for details of the calculation). The simulations were performed using a commercially available software, CST Microwave Studio, through a frequency domain solver (see supplementary material for details). As shown in Fig. 1(b), the electric dipole along *y*-axis (P_y) dominates the resonance in the vicinity of LC resonance frequency as a consequence of a strong electric excitation, which reveals a resonance with a small amplitude as well as a broad linewidth (quality factor, $Q \sim 3.1$ for the LC mode). Electric dipole along *x*-polarization (P_x) is also intensified due to the anisotropy with an asymmetric split gap. Although the planar configuration of metasurface does not allow the direct coupling of external magnetic component at normal incidence, the bianisotropic property of the ASRR enables an enhancement of magnetic dipole along the *z*-axis (M_z). Except the dominant electric and magnetic dipoles, all the other multipoles such as toroidal dipole ($T_{x,y}$),[31] electric and magnetic quadrupoles (Q^e, Q^m) exhibit much weaker scattered powers that have negligible influence on the LC resonance mode formed in the S1 arrangement.

The LC resonance has revealed numerous promising applications especially in sensing[40] due to its strong field confinement in the vicinity of the split gap and weak radiative loss. However, extremely weak coupling of the LC mode in ASRR with *y*-polarization leads to a marginal spectral footprint which is difficult to capture experimentally. A further reduction in the loss will give rise to an improved *Q* factor that in turn enables a better sensing performance of LC resonant metasurfaces. Here, in the uniform ASRR, a pronounced magnetic dipole provides a pathway to engineer the multipoles in a planar metasurface configuration by mirroring the neighboring resonators, which enables a relatively 180° phase shift for the time-harmonic magnetic dipole. We performed a detailed investigation on the amplitude and linewidth of the LC resonance in the transmission spectrum by engineering the orientation of neighboring resonators in the 2D metamaterial array, which introduces various contributions of composite multipoles in order to tailor the LC resonance.

The first arrangement is presented in Fig. 2(a), where the neighboring ASRR pair is mirrored with each other along the *y*-axis, and a supercell consisting of two resonators acts as a periodic composition named as S2. As revealed by the simulated surface current distributions in S1 and S2 with *y*-polarized incidence, the *in-phase* oscillation of current loops in the resonators of S1 configuration enables an enhancement of net magnetic dipole. However, the *anti-phase* oscillations of current loops in S2 configuration lead to the suppression of the magnetic dipole which gives rise to an in-plane toroidal dipole[41] along the *y*-axis, as illustrated in Fig. 2(b).

The transmission intensity of S2 is also measured with *y*-polarized incidence and plotted as the red line shown in Fig. 2(c). For a comparison, the corresponding spectrum of S1 is also plotted as a reference. We observe a strongly

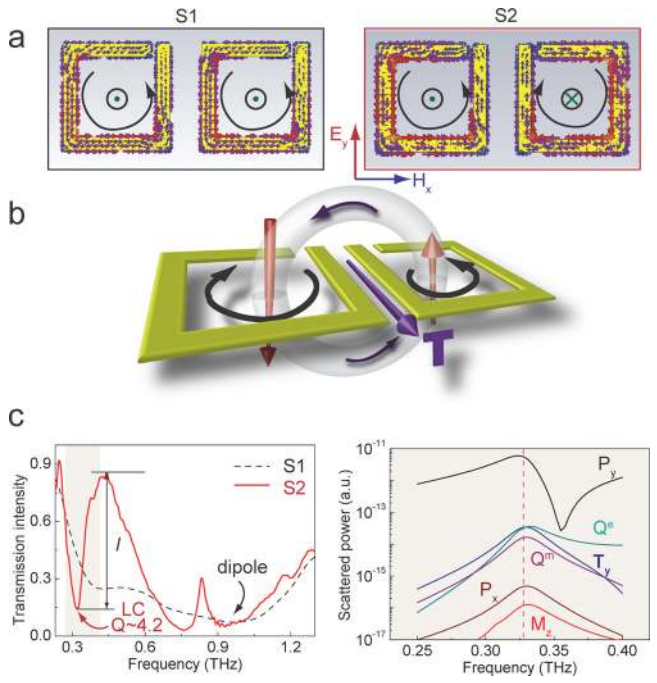

FIG. 2. Toroidal dipole excitation in a supercell by mirroring the neighboring ASRR pair. (a) Surface current distributions of S1 and S2 with *y*-polarized incidence. (b) Schematic illustration of in-plane toroidal dipole excitation in S2 due to the anti-phase magnetic dipoles. (c) Measured transmission intensity spectra of S1 and S2 with the calculated scattering power of multipoles of the LC mode in S2.

enhanced coupling of the LC mode to the free space with a dominant magnitude (I) in S2 that is numerically described by the dip to peak intensity in the transmittance spectrum. At dipole resonance, a new resonance mode emerges which is attributed to the onset of diffraction originating from the change in the lattice periodicity in the supercell S2.[42] In addition to the dramatic enhancement of the LC resonance, we also observe a redshift of the resonance in S2 due to the anti-phase magnetic dipoles that lower the resonant energy.[43] Meanwhile, Q factor of the engineered LC mode reveals a slight enhancement ($Q = 4.2$) as a consequence of the destructive interference of magnetic dipole and x-polarized electric dipole between the neighboring mirrored resonators that gives rise to an in-plane toroidal dipole (T_y), and accompanying magnetic quadrupole (Q^m), and electric quadrupole (Q^e), respectively. For a clearer numerical understanding of the intensified LC resonance, we plot the calculated multipole scattering power spectra of S2 in the vicinity of LC resonance on the basis of simulated current distributions as shown in Fig. 2(c). The predicted suppression of magnetic (M_z) and electric (x-polarized, P_x) dipoles is numerically verified by the multipole analysis, which in turn results in enhancement of the scattered power of toroidal dipole along the y-axis (T_y) and magnetic (Q^m) and electric quadrupoles (Q^e) in the planar configuration. The electric dipole along y-axis still plays a dominant role in the multipole decomposition, but with an enhanced resonance amplitude and narrower linewidth compared to those of S1, so that the LC resonance reveals an enhanced amplitude and Q factor. With the existence of mirror symmetry in the supercell configuration, the x-polarized component of electric dipole (P_x) is strongly suppressed which contributes to the weakening of the radiative losses.

The tailoring of main contribution from the scattered multipoles of the LC resonance is demonstrated by redistributing the resonators in the array which leads to a remarkable modulation of the eigen resonance linewidth and amplitude. By selectively pairing of the nearest neighbor resonators, the relative phase of the magnetic/electric dipoles is tailored in the planar supercell configuration. We then further broaden our horizon to different supercell configurations and discuss their resonance mode properties. For the case of S3 presented in Fig. 3(a), both horizontal and vertical neighboring magnetic dipoles undergo destructive interference with the mirrored resonators, which thus induces exactly opposing pairs of toroidal moments along the y-axis as well as x-axis with the mutually mirrored resonators, as shown in Fig. 3(a). In this case, one supercell comprises four mutually mirrored resonators, and the anti-phase surface currents not only cancel the magnetic dipole but also suppress the toroidal dipole. With only electric dipole along y-axis (P_y) scattered to the far-field, the resultant LC resonance reveals a further enhancement in Q factor (~4.9), as shown in Fig. 3(b). The scattered power from multipoles are calculated and presented in Fig. 3(c), where the suppression of electric (x-polarized, P_x), magnetic (M_z), and toroidal dipoles ($T_{x,y}$) is observed. In comparison to the case of S1, the LC resonance magnitude is enhanced with a larger coupling strength of electric dipole (P_y) to the far field. With the redistribution of the unit cells in the S3 array, the LC resonance frequency is further lowered.

With only the neighboring vertical resonators being mirrored in S4 as shown in Fig. 3(d), a toroidal dipole is expected to be enhanced along the x-axis with the suppressed magnetic and electric (x-polarized) dipoles. In this case, the measured LC resonance still possesses an enhanced magnitude relative to S1 with y-polarized incidence as shown in Fig. 3(e). The multipole analysis shown in Fig. 3(f) reveals that the magnetic dipole (M_z) is slightly weakened which leads to a relatively weaker enhancement of toroidal dipole along the x-axis (T_x). Since the vertical resonator pairs are not mirror symmetric along y-axis, the anti-phase magnetic dipole will not reveal a complete cancellation. Note that the electric dipole along y-axis still dominates the scattering power of multipoles, which determines the overall LC resonance property. Here, in S4, the scattered electric dipole (P_y) reveals the strongest resonance amplitude with a much narrower linewidth compared to all the other three cases due to the stronger confinement of energy inside the resonator array. As shown in Fig. 3(e), the LC resonance of S4 exhibits a Q factor of ~6.2 as well as a highly pronounced resonance intensity.

The improved Q factor of the LC resonance provides an excellent platform for ultrasensitive sensing due to the tight confinement of energy inside the resonator cavity which increases the lifetime of light-matter interaction. The Q factor is usually improved by reducing the losses in a system from two paths: radiative and nonradiative (Ohmic) losses. In terahertz regime, most metals, such as aluminum, behave as a nearly perfect conductor, and thus we only focus on

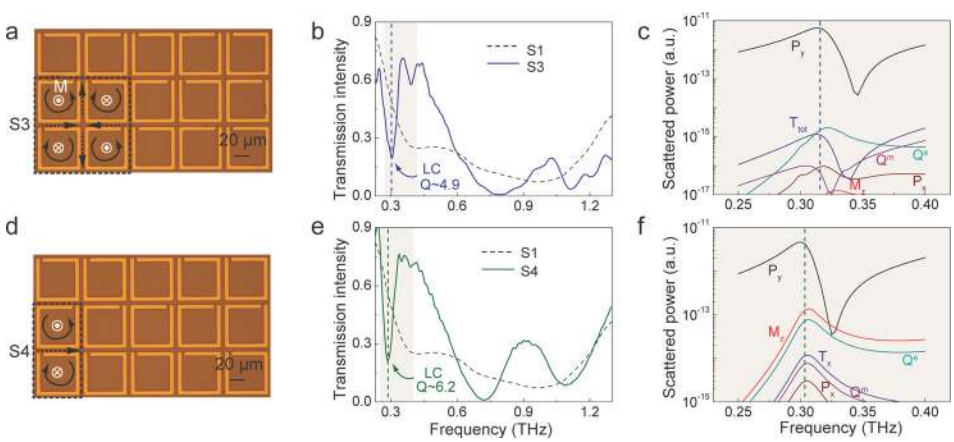

FIG. 3. Quality factor enhancement of LC resonance by rearranging the relative orientation of resonator pairs. (a) Sample image of S3, (b) measured transmission intensity spectra, and (c) calculated scattered power of multipoles for sample S3. (d)–(f) are the respective graphs for sample S4.

manipulating the radiative loss mechanism in this system. From the aspect of radiative loss, the commonly employed strategy is to induce a dark mode that weakly couples to free space such as a Fano resonance mode. However, weak coupling of the mode to free space results in a faint spectral signature that is difficult to measure in the far field. Therefore, there should be a tradeoff between the coupling coefficient and radiation decay rate of the resonance mode from an application perspective. Here, we define a figure of merit (FoM) to estimate this trade-off by calculating $FoM = Q \times I$, where Q is the quality factor indicating the decay rate and I is the resonant intensity indicating the coupling coefficient to the free space.[44]

To measure the performance of the multipole engineered LC resonances by redistributing the neighboring resonators in the 2D array, we calculate and summarize the spectral parameters from S1 to S4, as shown in Fig. 4. For S1, we show the Q factor and magnitude of LC resonance excited by x-polarized incidence for comparison, which reflects the intrinsic properties of this fundamental mode. From the graph in Fig. 4, there is a clear increasing trend for the Q factor from S1 to S4 by tailoring the respective multipoles, and the spectral resonance intensities are drastically enhanced from S1 configuration to S2, S3, and S4 configurations. According to the extraordinary performance of S2, S3, and S4 configurations, the FoMs of the LC resonances reveal abrupt improvements, and the best value exists at S4 configuration with an FoM of 3.4. Overall, the FoM of metamaterial samples S2 to S4 has improved compared to that of S1, which reveals the dominant role of multipoles in engineering the fundamental resonance mode. With the redistribution of resonators in the array, the respective resonant frequency (energy) of the LC resonance mode also shifts as indicated in Fig. 4.[43] Moreover, the performance could be further improved by tailoring the geometrical parameters of the resonator in order to reduce the radiative loss of the dominant electric dipole.

On the basis of the overall best spectral performance at S4 configuration, we picked up S4 design to elucidate the impact of the degree of asymmetry in ASRR. As shown in Fig. 5(a), the LC resonance for the S4 configuration was simulated for y-polarized incidence by changing the split gap displacement (d) of ASRR from the center. As the degree of

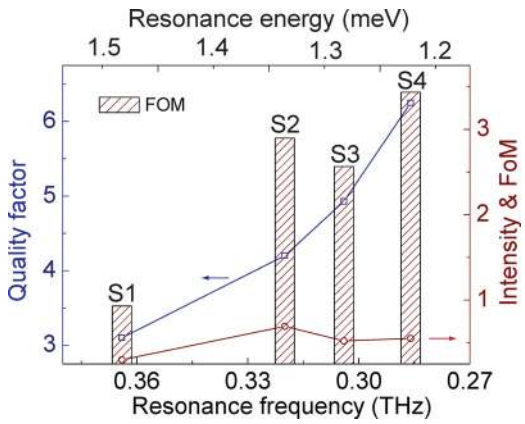

FIG. 4. Detailed performance parameters of the LC resonance for metamaterials S1, S2, S3, and S4 extracted from the experimental spectra.

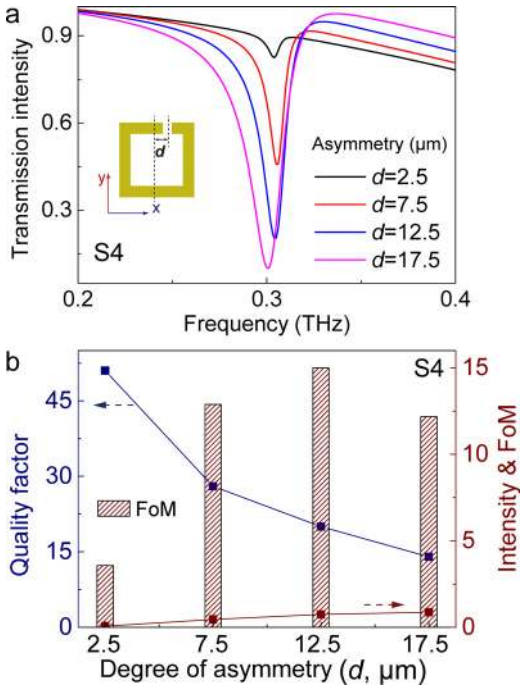

FIG. 5. Impact of the degree of asymmetry in ASRR for configuration of S4. (a) Simulated transmission spectra showing LC resonance evolution versus the degree of asymmetry d. (b) Retrieved quality factor, resonance intensity and FoM of LC resonance at different split gap displacements.

asymmetry was varied from $d = 2.5\ \mu$m to $d = 17.5\ \mu$m, the LC resonance shows a clear modulation in terms of Q factor as well as resonance intensity for the y-polarized excitation, which was not observed with x-polarized excitation (see supplementary material). The retrieved Q factor, resonance intensity and FoM are plotted in Fig. 5(b), where it clearly shows the resonance performance versus the change in the degree of asymmetry. The largest Q factor observed is 51 for $d = 2.5\ \mu$m. The highest FoM of 15 is observed for $d = 12.5\ \mu$m. In this context, we obtain the optimized performance of an ASRR array by engineering multipoles via the spatial arrangement of resonators as well as tailoring the intrinsic radiative loss of resonators via gap displacement.[40]

In summary, we have discussed the spectral properties of the LC resonance by engineering the multipoles in a single gap terahertz asymmetric split ring resonator array by spatial rearrangement of the neighboring resonators in a 2D metasurface. By tailoring the multipoles, the LC resonance undergoes an enormous change in its linewidth and intensity, followed by a shift of resonant frequency and an enhanced figure of merit. Controlling the LC resonance by manipulating the multipoles provides an alternative avenue to improve its application potential in biosensing, lasing spaser and nonlinear optics with an enhanced field confinement and large free-space coupling coefficient. This strategy of engineering the scattering power of multipoles just by spatial rearrangement in the array could be extended universally to most of the metamaterial and plasmonic systems in order to tailor the resonance modes, which would have a significant impact on optimizing the spectral performance of active as well as passive metadevices across a broad range of physical systems including electromagnetism, acoustics and thermal systems.

See supplementary material for the information on the numerical calculation of electromagnetic multipoles, simulation methods, and LC resonance modulation with *x*-polarized incidence.

The authors acknowledge the Singapore Ministry of Education Grant No. MOE2015-T2-2-103 for funding of this research.

[1]S. Linden, C. Enkrich, M. Wegener, J. Zhou, T. Koschny, and C. M. Soukoulis, Science **306**(5700), 1351–1353 (2004).
[2]D. R. Smith, J. B. Pendry, and M. C. Wiltshire, Science **305**(5685), 788–792 (2004).
[3]X. Ni, Z. J. Wong, M. Mrejen, Y. Wang, and X. Zhang, Science **349**(6254), 1310–1314 (2015).
[4]J. Li and C. Chan, Phys. Rev. E **70**(5), 055602(R) (2004).
[5]X. Liu, T. Tyler, T. Starr, A. F. Starr, N. M. Jokerst, and W. J. Padilla, Phys. Rev. Lett. **107**(4), 045901 (2011).
[6]T. Koschny, M. Kafesaki, E. N. Economou, and C. M. Soukoulis, Phys. Rev. Lett. **93**(10), 107402 (2004).
[7]B. Luk'yanchuk, N. I. Zheludev, S. A. Maier, N. J. Halas, P. Nordlander, H. Giessen, and C. T. Chong, Nat. Mater. **9**(9), 707–715 (2010).
[8]L. Cong, Y. K. Srivastava, A. Solanki, T. C. Sum, and R. Singh, ACS Photonics **4**(7), 1595–1601 (2017).
[9]I. Al-Naib, R. Singh, C. Rockstuhl, F. Lederer, S. Delprat, D. Rocheleau, M. Chaker, T. Ozaki, and R. Morandotti, Appl. Phys. Lett. **101**(7), 071108 (2012).
[10]M. Manjappa, Y. K. Srivastava, A. Solanki, A. Kumar, T. C. Sum, and R. Singh, "Hybrid Lead Halide Perovskites for Ultrasensitive Photoactive Switching in Terahertz Metamaterial Devices," Adv. Mater. (to be published).
[11]N. I. Landy, S. Sajuyigbe, J. J. Mock, D. R. Smith, and W. J. Padilla, Phys. Rev. Lett. **100**(20), 207402 (2008).
[12]L. Cong, W. Cao, X. Zhang, Z. Tian, J. Gu, R. Singh, J. Han, and W. Zhang, Appl. Phys. Lett. **103**(17), 171107 (2013).
[13]N. Yu, P. Genevet, M. A. Kats, F. Aieta, J. P. Tetienne, F. Capasso, and Z. Gaburro, Science **334**(6054), 333–337 (2011).
[14]L. Cong, P. Pitchappa, Y. Wu, L. Ke, C. Lee, N. Singh, H. Yang, and R. Singh, Adv. Opt. Mater. **5**(2), 1600716 (2017).
[15]N. Yu and F. Capasso, Nat. Mater. **13**(2), 139–150 (2014).
[16]G. Zheng, H. Mühlenbernd, M. Kenney, G. Li, T. Zentgraf, and S. Zhang, Nat. Nanotechnol. **10**(4), 308–312 (2015).
[17]T. Kaelberer, V. A. Fedotov, N. Papasimakis, D. P. Tsai, and N. I. Zheludev, Science **330**(6010), 1510–1512 (2010).
[18]Z.-G. Dong, P. Ni, J. Zhu, X. Yin, and X. Zhang, Opt. Express **20**(12), 13065–13070 (2012).
[19]M. J. Urban, P. K. Dutta, P. Wang, X. Duan, X. Shen, B. Ding, Y. Ke, and N. Liu, J. Am. Chem. Soc. **138**(17), 5495–5498 (2016).
[20]Z. Liu, S. Du, A. Cui, Z. Li, Y. Fan, S. Chen, W. Li, J. Li, and C. Gu, Adv. Mater. **29**(17), 1606298 (2017).
[21]T. A. Raybould, V. A. Fedotov, N. Papasimakis, I. Kuprov, I. J. Youngs, W. T. Chen, D. P. Tsai, and N. I. Zheludev, Phys. Rev. B **94**(3), 035119 (2016).
[22]I. B. Zel'Dovich, Sov. J. Exp. Theor. Phys. **6**, 1184 (1958).
[23]V. Flambaum and D. Murray, Phys. Rev. C **56**(3), 1641 (1997).
[24]A. Ceulemans, L. Chibotaru, and P. Fowler, Phys. Rev. Lett. **80**(9), 1861 (1998).
[25]V. Dubovik and V. Tugushev, Phys. Rep. **187**(4), 145–202 (1990).
[26]G. Afanasiev, J. Phys. D: Appl. Phys. **34**(4), 539 (2001).
[27]N. I. Zheludev, S. L. Prosvirnin, N. Papasimakis, and V. A. Fedotov, Nat. Photonics **2**(6), 351–354 (2008).
[28]Y. W. Huang, W. T. Chen, P. C. Wu, V. A. Fedotov, N. I. Zheludev, and D. P. Tsai, Sci. Rep. **3**, 1237 (2013).
[29]J. S. Totero Gongora, A. E. Miroshnichenko, Y. S. Kivshar, and A. Fratalocchi, Nat. Commun. **8**, 15535 (2017).
[30]X. Chen and W. Fan, Opt. Lett. **42**(10), 2034–2037 (2017).
[31]N. Papasimakis, V. A. Fedotov, V. Savinov, T. A. Raybould, and N. I. Zheludev, Nat. Mater. **15**(3), 263–271 (2016).
[32]J. Li, J. Shao, Y.-H. Wang, M.-J. Zhu, J.-Q. Li, and Z.-G. Dong, Opt. Express **23**(22), 29138–29144 (2015).
[33]M. Gupta and R. Singh, Adv. Opt. Mater. **4**(12), 2119–2125 (2016).
[34]M. Gupta, Y. K. Srivastava, M. Manjappa, and R. Singh, Appl. Phys. Lett. **110**(12), 121108 (2017).
[35]Y. Fan, Z. Wei, H. Li, H. Chen, and C. M. Soukoulis, Phys. Rev. B **87**(11), 115417 (2013).
[36]Y.-W. Huang, W. T. Chen, P. C. Wu, V. Fedotov, V. Savinov, Y. Z. Ho, Y.-F. Chau, N. I. Zheludev, and D. P. Tsai, Opt. Express **20**(2), 1760–1768 (2012).
[37]M. Gupta, V. Savinov, N. Xu, L. Cong, G. Dayal, S. Wang, W. Zhang, N. I. Zheludev, and R. Singh, Adv. Mater. **28**(37), 8206–8211 (2016).
[38]A. A. Basharin, V. Chuguevsky, N. Volsky, M. Kafesaki, and E. N. Economou, Phys. Rev. B **95**(3), 035104 (2017).
[39]M. V. Cojocari, K. I. Schegoleva, and A. A. Basharin, Opt. Lett. **42**(9), 1700–1703 (2017).
[40]J. F. O'Hara, R. Singh, I. Brener, E. Smirnova, J. Han, A. J. Taylor, and W. Zhang, Opt. Express **16**(3), 1786–1795 (2008).
[41]C. Ederer and N. A. Spaldin, Phys. Rev. B **76**(21), 214404 (2007).
[42]M. Manjappa, Y. K. Srivastava, and R. Singh, Phys. Rev. B **94**(16), 161103 (2016).
[43]N. Liu, S. Kaiser, and H. Giessen, Adv. Mater. **20**(23), 4521–4525 (2008).
[44]L. Cong, M. Manjappa, N. Xu, I. Al-Naib, W. Zhang, and R. Singh, Adv. Opt. Mater. **3**(11), 1537–1543 (2015).